JOURNAL OF COMPUTATIONAL PHYSICS 19, 339–352 (1975)

Theory of Plasma Simulation Using Multipole-Expansion Scheme

LIU CHEN AND HIDEO OKUDA

Plasma Physics Laboratory, Princeton University, Princeton, New Jersey 08540

Received January 7, 1975; revised February 6, 1975

Nonphysical grid effects in plasma simulation using the Multipole-Expansion scheme and Gaussian-shape charge particles are studied analytically in one dimension. General expressions for the linear dispersion relation, fluctuation spectra, energy, and momentum conservations are derived and then compared with those of the Cloud-in-Cell (CIC) scheme using cell-size clouds. The results indicate that the Dipole-Expansion scheme and its subtracted version have, in general, grid effects comparable to CIC. Grid effects, however, are greatly reduced in schemes keeping higher-order moments, such as the Quadrupole-Expansion scheme.

1. INTRODUCTION

Recently, Kruer, Dawson, and Rosen [1] have proposed the Multipole-Expansion (MPE) scheme for electrostatic plasma simulations with finite-size (extended) particles. According to this scheme, the moments of the charge density and the force are expanded about the nearest grid point. The above authors have used this scheme up to the dipole moment (Dipole-Expansion, DPE, scheme) in several one-dimensional problems, while Okuda and Dawson [2] applied it to study the plasma transport in multidimension. The results found using DPE are in general quite satisfactory. For example, the total energy is better conserved than in the Nearest-Grid-Point (NGP) scheme [3].

To determine the reliability of producing desirable physics, which is the most important property of plasma simulations, one has to examine the nonphysical properties associated with this scheme; notably, the grid effects [6, 7]. Although there is computational evidence that DPE also suffers from the usual grid instabilities with growth rate comparable to that of CIC or PIC [8], no systematic theory exists.

The purpose of the present work is to study the nonphysical grid effects in the MPE scheme and to compare them with the corresponding theory of Langdon for CIC and PIC schemes [7, 9]. This is quite useful, not only for providing better understandings of the MPE scheme, but also for comparison among various simulation schemes.

In the following sections, grid effects in the MPE scheme are investigated theoretically. For simplicity, we assume the simulation plasma to be infinite, uniform, and one-dimensional. There is no static magnetic field. Ions are immobile and form a neutralizing background. Since we are interested in the spatial grid effects, we assume the time to be continuous; i.e., we take the $\Delta t \to 0$ limit. Extensions to multidimensional, multicomponent, periodic, finite Δt or magnetized models are straightforward. In Section 2 a brief description of the algorithm is given. Assuming the simulation plasma is collisionless, linear dispersion relation correct to all moments of expansion is then derived and analyzed in Section 3. Comparisons are made between CIC, DPE, and the Quadrupole-Expansion (QPE) schemes. Section 4 contains derivations and discussions of the fluctuation spectra. Energy and momentum conservations are examined in Section 5. In Section 6, we analyze the Subtracted-Dipole-Expansion scheme, which is faster in field calculations than DPE. Final conclusions and discussion are given in Section 7.

2. Algorithm

The Multipole Expansion scheme works in the following way.

1. At each time step t, the moments of a charged particle with respect to its nearest grid point are first calculated. Let the ith particle be in the jth cell; i.e., $| x_i - x_j | \leqslant \Delta x/2$. Here x_i and $x_j = j\,\Delta x$ are the positions of the ith particle and the jth grid point, respectively. Δx is the grid spacing. The zeroth moment (monopole) is then given by

$$\rho_0(j, t) = \sum_{i \in j} 1, \tag{1}$$

the first moment (dipole) is

$$\rho_1(j, t) = \sum_{i \in j} [x_i(t) - x_j], \tag{2}$$

and the lth moment is

$$\rho_l(j, t) = \sum_{i \in j} [x_i(t) - x_j]^l. \tag{3}$$

2. As the second step, discrete Fourier transforms of $\rho_{gl}(x, t)$, $\rho_{gl}(k, t)$ are obtained. Here, $\rho_{gl}(x, t) = \sum_j \rho_l(j, t)\, \delta(x - x_j)$ is a function of the grid quantities ρ_l. Since the charge density $\rho(x, t)$ is given by

$$\rho(x, t) = q \sum_{l=0}^{\infty} \int dx' S(x - x') \frac{(-1)^l}{l!} \frac{d^l}{dx'^l} \rho_{gl}(x', t), \tag{4}$$

its Fourier transform for $| k \Delta x | \leqslant \pi$ can be written as

$$\rho(k, t) = qS(k) \sum_{l=0}^{\infty} \frac{(-ik)^l}{l!} \rho_{gl}(k, t), \tag{5}$$

where

$$S(k) = \exp[-(ka)^2/2] \tag{6}$$

is the shape factor of a Gaussian cloud with the "width" $2a$.

3. The third step is using Poisson's equation to obtain the Fourier transforms of the moments of force for $| k \Delta x | \leqslant \pi$;

$$F_0(k, t) = qS(k)\, E(k, t) \tag{7}$$

$$= -i4\pi qS(k)\, \rho(k, t)/k, \tag{7a}$$

and

$$F_l(k, t) = (ik)^l F_0(k, t). \tag{8}$$

4. Inverse discrete Fourier transform $F_l(k, t)$ to $F_l(j, t)$.

5. The last step is to calculate the force on the ith particle in the jth cell which is given by

$$F_{i \in j}(x_i, t) = \sum_{l=0}^{\infty} \frac{[x_i(t) - x_j]^l}{l!} F_l(j, t). \tag{9}$$

6. With $F(x_i, t)$ calculated, the ith particle is pushed forward to the next time step $t + \Delta t$ using the usual time-centered leap-frog particle pushing scheme.

3. Dispersion Relation

As the first step in analyzing the property of the MPE scheme, the dispersion relation is considered here. In order to obtain the linear dispersion relation, we analyze the particle dynamics using the algorithm described in the preceding section. Let us define the NGP weighting function, $\tilde{w}(x)$, as

$$\tilde{w}(x) = \begin{cases} 1/\Delta x, & | x | \leqslant \Delta x/2, \\ 0, & \text{otherwise.} \end{cases} \tag{10}$$

Then, the lth moment of the particle density is given by

$$\rho_l(j, t) = \Delta x \int_{-\infty}^{\infty} dx' (x' - x_j)^l \tilde{w}(| x_j - x' |)\, n(x', t), \tag{11}$$

where

$$n(x, t) = \sum_{i=1}^{N} \delta[x - x_i(t)] \tag{12}$$

is the microscopic particle density and N is the total number of particles. Note that for an infinite system we require that as N and L (system length) become infinite, the average uniform density $n_0 = N/L$ stay finite. Now for $\rho_{gl}(x, t)$ defined as

$$\rho_{gl}(x, t) = \sum_{j=-\infty}^{\infty} \rho_l(j, t)\, \delta(x - x_j), \tag{13}$$

its (spatial) Fourier transform is

$$\rho_{gl}(k, t) = \sum_{p=-\infty}^{\infty} (-i)^l\, w^{(l)}(k_p)\, n(k_p, t), \tag{14}$$

where

$$w(k) = \sin(k\, \Delta x/2)/(k\, \Delta x/2), \tag{15}$$

$w^{(l)}(k) = d^l w(k)/dk^l$, $k_p = k - pk_g$, and $k_g = 2\pi/\Delta x$. Poisson's sum formula [10] is used to derive Eq. (14). Substituting Eq. (14) into Eq. (5), we have for $| k\, \Delta x | \leqslant \pi$,

$$\rho(k, t) = qS(k) \sum_{p} I(k, k_p)\, n(k_p, t), \tag{16}$$

and

$$I(y, z) = \sum_{l=0}^{\infty} \frac{(-y)^l}{l!}\, w^{(l)}(z). \tag{17}$$

It is understood that the sum of p runs from $-\infty$ to ∞.

For the grid force functions, we define

$$F_{gl}(x, t) = \sum_{j=-\infty}^{\infty} F_l(j, t)\, \delta(x - x_j). \tag{18}$$

From Eq. (9), the force felt by a particle at x is then given by

$$F(x, t) = \Delta x \sum_{l=0}^{\infty} \int dx' \frac{(x - x')^l}{l!}\, \tilde{w}(| x - x' |)\, F_{gl}(x', t). \tag{19}$$

The Fourier transform of $F(x, t)$ is

$$F(k, t) = \Delta x \sum_{l=0}^{\infty} \frac{(i)^l}{l!}\, w^{(l)}(k)\, F_{gl}(k, t). \tag{20}$$

Now if one defines $F_l(k, t)$, Eq. (8), to be a periodic function in k with the periodicity k_g, $F_{gl}(k, t)$ is then by

$$F_{gl}(k, t) = \frac{1}{\Delta x} F_l(k, t) = \frac{1}{\Delta x} (ik)^l F_0(k, t), \tag{21}$$

and

$$F_{gl}(k + pk_g, t) = F_{gl}(k, t). \tag{22}$$

Now, in order to obtain the linear dispersion relation, we assume that the simulation plasma is collisionless (Vlasov) and that time is continuous. Then the force and density perturbation are related through the Vlasov equation. In the linear regime we obtain for the perturbed density $n_1(x, t)$,

$$n_1(k, \omega) = -i(n_0/m)\, \psi(k, \omega)\, F(k, \omega), \tag{23}$$

where

$$\psi(k, \omega) = \int \frac{df_0/dv}{\omega - kv}\, dv. \tag{24}$$

$f_0(v)$ is the equilibrium velocity distribution function, and $\operatorname{Im} \omega \geqslant 0$ for the Laplace transform in time. From Eqs. (7a), (16), and (20)–(23), and note $n(k, \omega) = 2\pi n_0\, \delta(k) + n_1(k, \omega)$, we find for $k \neq 0$ and $| k\, \Delta x | \leqslant \pi$,

$$\rho(k) = -\omega_p^2 \frac{S^2(k)}{k} \sum_p I^2(k, k_p)\, \psi(k_p, \omega)\, \rho(k). \tag{25}$$

ω_p is the plasma frequency. The linear dispersion relation for $| k\, \Delta x | \leqslant \pi$ is then

$$\epsilon(k, \omega) = 1 + \omega_p^2 [S^2(k)/k] \sum I^2(k, k_p)\, \psi(k_p, \omega), \qquad \operatorname{Im} \omega \geqslant 0. \tag{26}$$

For $|(k - rk_g)\, \Delta x | \leqslant \pi$, one simply replaces k in Eq. (26) by kr to obtain the corresponding dispersion relation. For comparison, the dispersion relation of the standard charge-sharing scheme is [7]

$$\tilde{\epsilon}(k, \omega) = 1 + (\omega_p^2/\kappa) \sum_p | w^2(k_p)|^\alpha\, \psi(k_p, \omega), \qquad \operatorname{Im} \omega \geqslant 0. \tag{27}$$

Here, $\alpha = 1$ for NGP and $\alpha = 2$ for CIC or PIC with cloud size Δx. κ is a function of k and is related to the Poisson solver. For example, $\kappa = \tan(k\, \Delta x/2)(\Delta x/2)^{-1}$ when a finite differencing scheme is used for Poisson's equation. There is, however, freedom in choosing the form of κ within the first Brillouin zone, $| k\, \Delta x | \leqslant \pi$, so that the desired physics can be best achieved [7]. By comparing the forms of ϵ and $\tilde{\epsilon}$, one can easily see that the MPE scheme has the usual grid instabilities; e.g.,

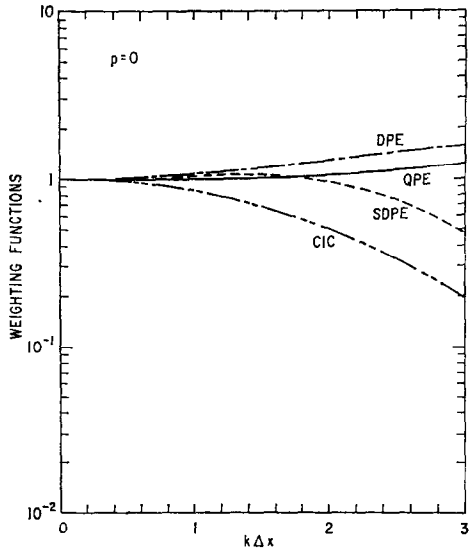

FIG. 1. Plot of weighting functions, I^2, with $p = 0$ for DPE, SDPE, QPE, and CIC schemes. The clouds in CIC are of cell size.

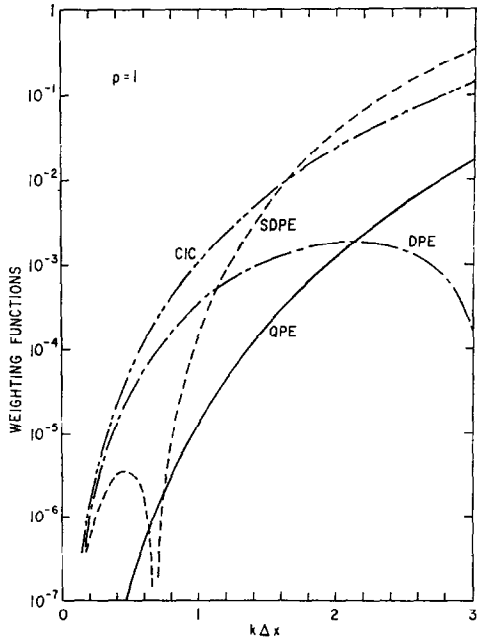

FIG. 2. Plot of weighting functions, I^2, with $p = 1$ for DPE, SDPE, QPE, and CIC schemes. The clouds in CIC are of cell size.

in a stationary Maxwellian with $\lambda_D/\Delta x \sim 0.1$, as the charge-sharing schemes [6, 7, 8].

To examine quantitatively the grid effects in the MPE scheme, the weighting functions, I^2 in Eq. (26), corresponding to DPE and QPE are numerically evaluated for $k\,\Delta x = 0.1$ to 3.0 and $p = 0, \pm 1, \pm 2$. The expressions of the weighting functions are

$$I_M^2(k, k_p) = \left[\sum_{l=0}^{l_M} \frac{(-k)^l}{l!} w^{(l)}(k_p)\right]^2. \tag{28}$$

Here, $M = D$, $l_D = 1$ for DPE and $M = Q$, $l_Q = 2$ for QPE. For comparison, similar evaluations are carried out for the weighting function of CIC with cell-size clouds, which is given by

$$I_C^2(k, k_p) = w^4(k, k_p). \tag{29}$$

The results are shown in Figs. 1–5. Because in the CIC scheme one often practices additional **k**-space smoothings to suppress the short-wavelength ($|k\,\Delta x| \gtrsim 1$) modes, the Gaussian shape factor, which has similar effects, is, therefore, not

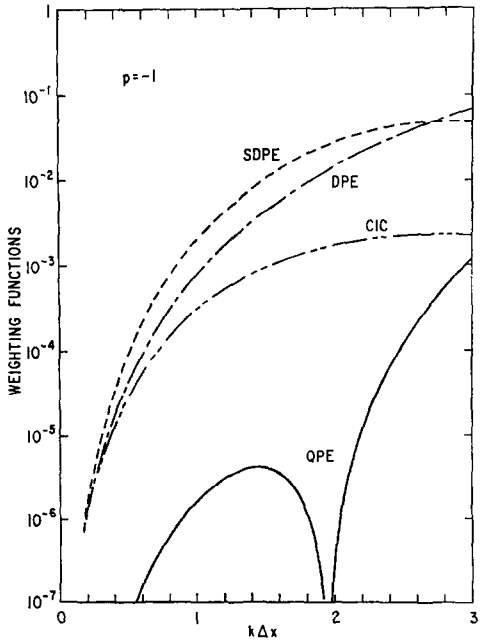

FIG. 3. Plot of weighting functions, I^2, with $p = -1$ for DPE, SDPE, QPE, and CIC schemes. The clouds in CIC are of cell size.

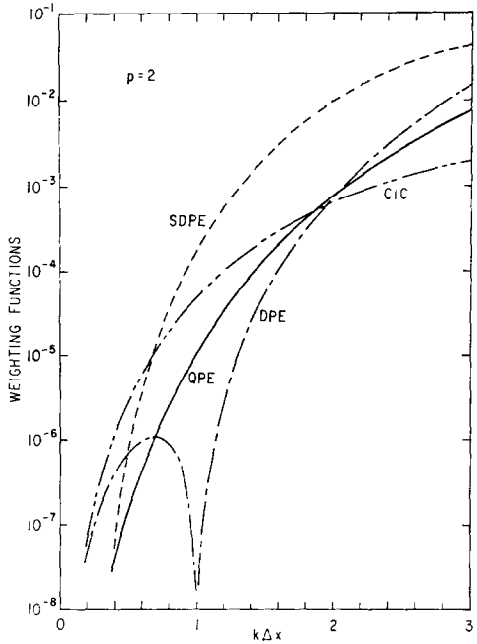

FIG. 4. Plot of weighting functions, I^2, with $p = 2$ for DPE, SDPE, QPE, and CIC schemes. The clouds in CIC are of cell size.

introduced into the weighting functions of the MPE scheme. Furthermore, since only the long-wavelength ($| k \Delta x | < 1$) modes are of physical interest, we concentrate our discussions on this regime.

Figure 1 plots the weighting functions of the various schemes for $p = 0$; i.e., they correspond to the dynamics produced by the forces averaged over the grid points. For $| k \Delta x | < 1$, similar to CIC, $I_D^2 \simeq I_Q^2 \simeq 1$, which gives us confidence in the capabilities of the schemes to produce the desired physics in the long-wavelength regime. It should be noted, however, that these curves do not help one choose between CIC and the MPE schemes.

The grid alias effects are shown in Figs. 2–5, where the weighting functions of the various schemes are plotted for $p = \pm 1$ and ± 2. In general, for $| k \Delta x | < 1$, the grid alias effects of DPE and CIC with cell-size clouds are comparable; consistent with simulation results [8]. The QPE scheme, which includes one higher moment of expansion and, therefore, involves additional computational work significantly reduces the grid alias effects. Note, however, CIC using more sophisticated particles (e.g., the parabolic spline) has also been practiced successfully to reduce the alias effects.

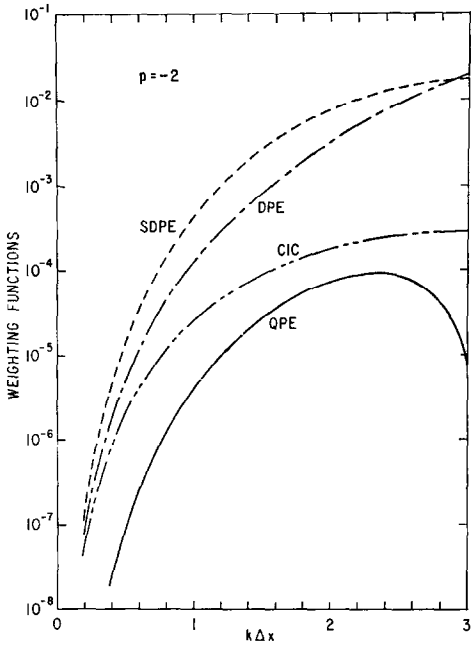

FIG. 5. Plot of weighting functions, I^2, with $p = -2$ for DPE, SDPE, QPE, and CIC schemes. The clouds in CIC are of cell size.

4. FLUCTUATION SPECTRUM

Let us consider a homogeneous, stationary, and stable (physically as well as nonphysically) ensemble of simulation plasmas. Using Eq. (16), and the well-known result of density fluctuation in a plasma, the spectrum of charge density fluctuation for MPE and $| k \Delta x | \leqslant \pi$ can be readily obtained as

$$(\rho^2)_{k,\omega} = \frac{2\pi n_0 q^2 S^2(k)}{| \epsilon(k, \omega)|^2} \sum_p I^2(k, k_p) \int dv f_0(v)\, \delta(\omega - k_p v). \tag{30}$$

The electric field fluctuation spectrum then is

$$(E^2)_{k,\omega} = (4\pi/k)^2 (\rho^2)_{k,\omega}\,. \tag{31}$$

As a comparison, the corresponding expression for CIC with cell-size clouds is [9]

$$(\tilde{E}^2)_{k,\omega} = (4\pi/\kappa)^2 \frac{2\pi n_0 q^2}{| \tilde{\epsilon}(k, \omega)|^2} \sum_p W^4(k_p) \int dv f_0(v)\, \delta(\omega - k_p v). \tag{32}$$

Thus both spectra essentially yield the gridless spectra for $| k \Delta x | < 1$.

We can also find the force fluctuation spectrum from Eqs. (7), (20), (21), and (31); i.e.,

$$(F^2)_{k,\omega} = q^2 I^2(k, k)\, S^2(k) (E^2)_{k,\omega}\,. \tag{33}$$

Using $(F^2)_{k,\omega}$, a corresponding Balescu–Lenard kinetic equation can be constructed following the method of Langdon for the charge-sharing scheme [9]. This is straightforward and we will not go into it here.

5. Energy and Momentum Conservations

Since the check on energy and momentum conservations is always an assurance of good physics and is being widely used, we examine it here for the MPE scheme. The time rate of change in the field energy is given by

$$\frac{d}{dt}(F.E.) = \frac{d}{dt}\frac{1}{16\pi^2}\int_{-k_g/2}^{k_g/2} dk\, |\, E(k, t)|^2$$

$$= -\frac{1}{2\pi}\sum_p \int_{-k_g/2}^{k_g/2} dk\, S(k)\, I(k, k_p)\, E(k, t)\, J(-k_p\,, t)\, k_p/k. \tag{34}$$

Here, $J(k, t)$ is the current density. In deriving Eq. (34), we have used Poisson's equation, Eq. (16), and the continuity equation. Now, the time rate of change in the kinetic energy is given by

$$\frac{d}{dt} K.E. = \frac{1}{2\pi}\int_{-\infty}^{\infty} dk\, \frac{F(k, t)}{q}\, J(-k, t), \tag{35}$$

which becomes, with Eqs. (7) and (20)–(22),

$$\frac{d}{dt} K.E. = \frac{1}{2\pi}\sum_p \int_{-k_g/2}^{k_g/2} dk\, S(k)\, I(k, k_p)\, E(k, t)\, J(-k_p\,, t). \tag{36}$$

Combining Eqs. (34) and (36), we have

$$\frac{d}{dt}(T.E.) = \frac{1}{2\pi}\sum_{p\neq 0} \int_{-k_g/2}^{k_g/2} dk S(k)\, I(k, k_p)\, E(k, t)\, J(-k_p\,, t)(1 - k_p/k). \tag{37}$$

Note that $k_p = k$ for $p = 0$. Thus, energy is not conserved due to the presence of the grid aliases ($p \neq 0$ terms) as in the CIC scheme.

As to the momentum, it is conserved (not so obviously) for the MPE as well as for charge-sharing schemes. The proof is given in the Appendix.

6. Subtracted-Dipole-Expansion Scheme

In order to reduce the number of Fourier and Inverse Fourier transforms required in the standard DPE scheme (four times in one dimension), Kruer *et al.* [1] proposed an alternative algorithm, the Subtracted-Dipole-Expansion (SDPE) scheme, which requires only two transforms in one dimension; i.e., the same as in NGP. SDPE differs from DPE in that the derivatives are replaced by the difference between the neighboring grid points. That is, in charge density calculation we have at each grid point an effective grid charge

$$\rho_e(j, t) = \rho_0(j, t) - [\rho_1(j + 1, t) - \rho_1(j - 1, t)]/2\Delta x. \tag{38}$$

The corresponding $\rho(k, t)$ for $| k \Delta x | \leqslant \pi$ then is given by

$$\rho_{SD}(k, t) = qS(k)\, \rho_{ge}(k, t), \tag{39}$$

where $\rho_{ge}(x, t) = \sum_j \rho_e(j, t)\, \delta(x - x_j)$. As in DPE, we obtain $F_0(k, t)$ for $| k \Delta x | \leqslant \pi$ and, hence, $F_0(j, t)$ from $\rho_{SD}(k, t)$ using Eq. (7). The force felt by the ith particle in the jth cell, however, is modified to

$$F_{i \in j}(x_i) = F_0(j, t) + (x_i - x_j)[F_0(j + 1, t) - F_0(j - 1, t)]/2\, \Delta x. \tag{40}$$

Since this scheme is faster than DPE in field calculations and appears to give satisfactory results [1], it is worthwhile to examine SDPE in more detail. In the following, we derive the corresponding dispersion relation and discuss its grid properties with respect to other schemes. The analyses are similar to those in Section 3.

From Eq. (38), $\rho_{ge}(k, t)$ can be shown to be

$$\rho_{ge}(k, t) = \rho_{g0}(k, t) - ikw(2k)\, \rho_{g1}(k, t). \tag{41}$$

Using Eq. (14) for ρ_{g0} and ρ_{g1} in Eq. (41), Eq. (39) reduces to

$$\rho_{SD}(k, t) = qS(k) \sum_p I_{SD}(k, k_p)\, n(k_p, t), \tag{42}$$

where

$$I_{SD}(y, z) = w(z) - yw(2y)\, w^{(1)}(z). \tag{43}$$

Similarly to Eq. (20) we find, for the force,

$$F(k, t) = \Delta x \sum_{l=0}^{1} \frac{(i)^l}{l!}\, w^{(l)}(k)\, F_{gl}(k, t), \tag{44}$$

where

$$F_{gl}(k, t) = F_{gl}(k + pk_g)$$
$$= \frac{1}{\Delta x}(ik)^l [w(2k)]^l F_0(k, t). \tag{45}$$

Combining Eqs. (7a), (23), (42), (44), and (45), we obtain the linear dispersion relation for $| k \Delta x | \leqslant \pi$,

$$\epsilon_{SD}(k, \omega) = 1 + \omega_p{}^2 \frac{S^2(k)}{k} \sum_p I_{SD}^2(k, k_p)\, \psi(k_p, \omega), \qquad \text{Im } \omega \geqslant 0. \tag{46}$$

Equation (46) indicates that the usual grid instability, again, would occur in SDPE. To compare the grid effects with those in other schemes, we compute, similarly, I_{SD}^2 for $p = 0, \pm 1$, and ± 2 over the same range of $k \Delta x$, from 0.2 to 3.0. The results are also shown in Figs. 1–5. Again, we concentrate on the physically important long-wavelength ($| k \Delta x | < 1$) modes. These plots indicate that for $| k \Delta x | < 1$ the grid effects in SPDE are comparable to those in DPE and CIC. Since SPDE is computationally faster than DPE, our results suggest that SDPE is preferable to DPE. Although we have only analyzed the Subtracted-Dipole case, the above analyses can be extended to include the higher moments.

7. Conclusions and Discussion

In the previous sections, using a one-dimensional model, we have theoretically analyzed the Multipole-Expansion simulation scheme proposed by Kruer *et al.* [1], and compared it with other schemes. A linear dispersion relation correct for all moments of expansion is derived, which shows the existence of nonphysical grid effects. Comparison of grid effects in CIC with cell-size clouds, DPE, and QPE indicate that for long-wavelength ($| k \Delta x | < 1$), where the physics is most important, the grid effects in CIC and DPE are comparable, but larger than those in QPE. We also derive expressions of fluctuations in the MPE scheme. We demonstrate that, similar to CIC, for MPE the total energy is not conserved due to the alias effects ($p \neq 0$ terms). The MPE scheme, however, conserves the total momentum as in the CIC scheme.

We also examine the Subtracted-Dipole-Expansion scheme, which reduces the number of Fourier transforms required in DPE and, hence, is faster in field calculations than DPE. The corresponding dispersion relation is derived and analyzed. For $| k \Delta x | < 1$, grid effects are comparable to CIC and DPE.

The above results, thus, suggest that nonphysical grid effects associated with the MPE and the Subtracted-MPE schemes, such as DPE and SDPE, are in general

comparable to those in CIC. Note that in the present work we have treated the one-dimensional case. Although we expect similar properties in higher dimensions, exact analyses are needed in the future.

As we have shown, by keeping higher moments in the multipole expansion, grid effects can be greatly reduced in the long-wavelength ($| k \Delta x | < 1$) regime, which is generally the most important regime of physical interest. Thus, it appears that the MPE scheme can also be used to reduce the grid effects and, therefore, in producing the desired physics. As remarked before, comparisons between the MPE and spline schemes involving similar amounts of computation remain to be worked out.

One of the examples which require the high accuracy of electric field calculations is the two-dimensional guiding center model in a strong magnetic field [11]. The particle motion is approximated as being a massless guiding center in this model and, therefore, there is no kinetic energy associated with particles. The electric field calculations then determine the accuracy of the evolution of the system and so it is essential to have highly accurate computation when determining the irreversible transport processes such as particle diffusion in this guiding center model. Unfortunately, it is known [12] that the standard charge-sharing scheme fails to maintain a sufficiently high accuracy of computation for a long period of time, while one could expect the higher-order MPE scheme, such as QPE, or CIC with more sophisticated particles, such as parabolic spline, to save the situation.

Recently, Chen, Langdon, and Birdsall [13] proposed grid "jiggling" and "interlacing" schemes in order to reduce the grid effects in charge-sharing schemes, such as CIC. They found that "jiggling" produces nonphysical high-frequency ($\sim \Delta t^{-1}$) modes which can be either stable or unstable depending on the velocity distribution. "Interlacing" eliminated certain groups of aliases and has no such ill effects. It requires, however, that the particles be processed at least twice in each time step and, hence, is computationally expensive. Although it is hard to compare quantitatively the reduction factors in the "interlacing" and MPE schemes, the MPE, while limited by the required grid storage, seems more attractive from the computational point of view.

APPENDIX

Momentum conservation. Here we prove that the total momentum is conserved in the MPE scheme. As usual, the time rate of change in the total momentum is given by

$$\frac{d}{dt} T.M. = \frac{1}{2\pi} \cdot \frac{1}{m} \int_{-\infty}^{\infty} dk\, F(k, t)\, n(-k, t). \tag{A.1}$$

Using Eqs. (7a), (16), and (20)–(22), Eq. (A.1) becomes

$$\frac{d}{dt} T.M. = -\frac{i}{2\pi n_0} \omega_p^2 \int_{-k_g/2}^{k_g/2} \sum_{p,r} dk\, n(-k_p, t)\, n(k_r, t)\, I(k, k_p)\, I(k, k_r)\, S^2(k)/k. \tag{A.2}$$

It is easy to show that the integrand is an odd function in k. Hence, we have

$$\frac{d}{dt} T.M. = 0. \tag{A.3}$$

ACKNOWLEDGMENT

The authors are grateful to A. Bruce Langdon for his valuable comments. This work was supported by U. S. Atomic Energy Commission Contract E(11-1)-3073.

REFERENCES

1. W. L. KRUER, J. M. DAWSON, AND B. ROSEN, *J. Computational Phys.* **13** (1973), 114.
2. H. OKUDA AND J. M. DAWSON, *Phys. Fluids* **16** (1973), 1408.
3. S. P. YU, G. P. KOOYERS, AND O. BUNEMAN, *J. Appl. Phys.* **36** (1965), 2550.
4. C. K. BIRDSALL AND D. FUSS, *J. Computational Phys.* **3** (1969), 494.
5. R. L. MORSE AND C. W. NIELSON, *Phys. Fluids* **12** (1969), 2418.
6. E. L. LINDMAN, *J. Computational Phys.* **5** (1970), 13.
7. A. B. LANGDON, *J. Computational Phys.* **6** (1970), 247.
8. H. OKUDA, *J. Computational Phys.* **10** (1972), 475.
9. A. B. LANGDON, in "Proceedings of the Fourth Annual Conference on Numerical Simulation of Plasmas" (1970), U.S. Government Printing Office, Washington, D.C. 20402, Stock No. 08510059.
10. P. M. MORSE AND H. FESHBACH, "Methods of Theoretical Physics," Chap. 4, p. 467, McGraw–Hill, New York/Toronto/London, 1953.
11. J. B. TAYLOR AND B. MCNAMARA, *Phys. Fluids* **14** (1971), 1492.
12. J. CHRISTEANSEN AND J. B. TAYLOR, *Plasma Phys.* **15** (1973), 585.
13. L. CHEN, A. B. LANGDON, AND C. K. BIRDSALL, *J. Computational Phys.* **14** (1974), 200.